



Mechanics of axisymmetric wavy surface adhesion: JKR–DMT transition solution

J.F. Waters^a, S. Lee^b, P.R. Guduru^{a,*}

^a Division of Engineering, Brown University, Providence, RI 02912, USA

^b The Boeing Company, Seattle, WA 98124, USA

ARTICLE INFO

Article history:

Received 2 April 2007

Received in revised form 3 April 2008

Available online 1 November 2008

Keywords:

Contact mechanics

Adhesion

Wavy surface

JKR–DMT transition

ABSTRACT

Recent work on the mechanics of detachment of a rigid sphere from an elastic axisymmetric wavy surface in the presence of JKR adhesion has shown that the presence of small-amplitude waviness introduces instabilities into the detachment process which dissipate mechanical energy. These instabilities result in interface toughening and strengthening; both the external work and peak force required for separation of a wavy interface are higher than those for a flat interface. In this paper, we summarize the key dimensionless parameters governing axisymmetric wavy surface adhesion in the JKR regime. We then proceed to derive a solution for the JKR–DMT adhesion transition for the axisymmetric wavy surface contact problem using a Maugis–Dugdale cohesive zone formulation. The phenomenon of interface toughening and strengthening due to the presence of surface waviness is seen to be restricted primarily to the JKR adhesion regime.

© 2008 Elsevier Ltd. All rights reserved.

1. Introduction

Traditionally, surface roughness has been viewed as reducing adhesion between elastic solids. This makes intuitive sense for relatively stiff materials, as roughness prevents intimate surface contact. Thus, as most naturally occurring surfaces are somewhat rough, the vast majority of engineering materials do not appear to adhere to each other at all at macroscopic length scales.

However, biologists have been aware for some time of instances where surface roughness is found to enhance adhesion. For example, in studies on the adhesion of marine invertebrates, Walker (1987) observed that adult tubeworms demonstrate significant adhesion to rough slate but minimal adhesion to smooth surfaces, and that barnacles also show a significant increase in tenacity to roughened surfaces. More recently, Santos et al. (2005) investigated the adhesion of echinoderm tube feet and observed higher tenacity on roughened polymer surfaces than on smooth surfaces. In the latter study, scanning electron microscopy confirmed deformation of the soft tube feet to match the profile of the rough substrate, and this effective increase in the true area of contact was proposed to explain the enhanced adhesion to rough surfaces.

Studies of the adhesion of rubbers and other soft elastomeric materials, similar to those commonly found in biological adhesion mechanisms, have also provided evidence for stronger adhesion to slightly roughened surfaces than to smooth ones. Experiments by Briggs and Briscoe (1977), Fuller and Roberts (1981), and Kim

and Russell (2001) on elastomers in contact with roughened rigid surfaces showed that the maximum pull-off force and detachment energy increased with roughness amplitude and reached a maximum before decreasing.

Most mechanical models of rough surface contact and adhesion have failed to satisfactorily predict or explain this phenomenon. Fuller and Tabor (1975) first derived a solution for the JKR adhesion (Johnson et al., 1971) of rough surfaces using the Greenwood and Williamson (1966) model, which assumes a Gaussian height distribution of noninteracting spherical asperities with uniform radii. Although the JKR theory is well-suited for modeling the adhesion of the compliant elastic materials which demonstrate the phenomenon, both the Fuller and Tabor model, and a more detailed derivation presented by Fuller and Roberts (1981) to attempt to explain their experimental results, failed to predict any increase of adhesion over that on a smooth surface. Fractal surface models have been used extensively by Persson and Tosatti (2001) and Persson (2002) to study rough surface adhesion, and these models do in fact predict an increase in net energy required to separate a unit area of rough interface. As in the case of the biological adhesion study of Santos et al. (2005), this increase in adhesion is attributed to an effective increase in the true area of contact for compliant materials in contact with surfaces having small amplitude roughness. However, the Persson models use an energy balance approach which assumes that attachment and detachment are completely reversible processes, which is not physically realistic.

The topic of rough surface adhesion has become increasingly important in the areas of nano- and micro-tribology, as surface forces become dominant when the size scale of contacting bodies

* Corresponding author. Tel.: +1 401 863 3362; fax: +1 401 863 9009.

E-mail address: pradeep_guduru@brown.edu (P.R. Guduru).

becomes small, and surface roughness plays an increasingly large role in determining the adherence between two bodies. However, below a certain length scale of contact, the assumptions in the JKR theory of adhesion begin to break down. Thus, to study nano-scale roughness effects on adhesion, the analytic model proposed by Maugis (1992) to capture the transition from the JKR regime to the DMT (Derjaguin et al., 1975) adhesion theory, which is more suitable for stiff materials and small length scales, is often used. The Maugis model uses a Dugdale cohesive zone formulation to approximate the effect of surface forces acting outside the area of contact. Recently, this model of the JKR–DMT adhesion transition has been incorporated into a Greenwood–Williamson rough surface contact model (Morrow et al., 2003) as an extension of the work of Fuller and Tabor (1975), as well as a fractal rough surface contact model (Morrow and Lovell, 2005), similar to that used in the work of Persson. Interestingly, in the work of Morrow et al. (2003), the adherence force is seen to steadily decrease as a function of a dimensionless roughness parameter, but enhanced adhesion below a critical roughness parameter is observed in the work of Morrow and Lovell (2005). This disparity in the predictions of the JKR–DMT adhesion transition models, in addition to the conflicting predictions for rough surfaces in the JKR models mentioned above, demonstrate the need for a more thorough understanding of how slightly rough surfaces can generate the enhanced adherence which is observed experimentally.

One method of developing such an understanding is to study rough surface contact mechanics using simplified surface geometries. Sinusoidal wavy surfaces lend themselves to exact analytic solutions, and have been used in several previous studies to approximate rough surfaces. Johnson (1995) first considered the planar wavy surface problem with JKR adhesion and derived the pressure necessary for surfaces to come into full contact. Hui et al. (2001), Carbone and Mangialardi (2004), and Zilberman and Persson (2002) also studied sinusoidal planar surfaces using various approaches. Each of these papers focuses primarily on partial contact and the conditions necessary for the two surfaces to jump into full contact during approach. However, recently the work of Guduru (2007) and Guduru and Bull (2007) has shown that the detachment process is more relevant in terms of understanding how small amplitude surface waviness can enhance adhesion. Guduru (2007) studied the mechanics of detachment of a rigid sphere from an elastic axisymmetric wavy surface in the presence of JKR adhesion and demonstrated how the presence of waviness introduces oscillations in the equilibrium force–penetration curves which amplify the tensile force required to separate the surfaces, causing interface strengthening. Further, these same oscillations introduce instabilities into the detachment process which dissipate mechanical energy, resulting in interface toughening. Detachment experiments performed on gelatin by Guduru and Bull (2007) demonstrated these phenomena and confirmed the experimental model. Thus, the force amplifications and irreversible dissipation of energy during the separation process suggest that the adhesion enhancement seen for soft elastomers on slightly rough surfaces is not due solely to the increase in effective contact area as proposed by other authors. As noted by Hui et al. (2001), most real surfaces have asperities which are in close enough proximity to interact elastically, and thus do not behave like surfaces comprised of isolated JKR spherical asperities, as is commonly assumed in most models. Allowing for asperity interaction in rough surface adhesion models appears to be critical for properly capturing the instabilities and energy dissipation seen in the work of Guduru (2007).

The purpose of this article is to further explore the mechanisms for interface toughening and strengthening of adhesive wavy surfaces, and provide physical insights into how existing models for more realistic rough surfaces might be improved to better capture

such phenomena. The paper is organized as follows. First, taking advantage of canonical exact analytical solutions for axisymmetric contact problems, the JKR solution for the axisymmetric wavy surface contact problem is discussed, and presented in a new dimensionless form which allows comprehensive adhesion maps to be drawn. Then, the JKR–DMT transition solution is derived using a Maugis–Dugdale cohesive zone formulation, and the enhancement in adhesion due to surface waviness is mapped. The phenomena of interface toughening and strengthening are highlighted for both the JKR and JKR–DMT transition solutions. Significant enhancement in adhesion due to the presence of a slightly wavy surface is observed, and it is seen that most of this enhancement is limited to the JKR adhesion regime.

2. Axisymmetric wavy surface adhesion: JKR theory

2.1. Wavy surface geometry

As a simple approximation to the rough surface contact problem, we consider contact between a rigid spherical indenter and the axisymmetric wavy surface of a linearly elastic half-space. The wavy surface is described as a sinusoidal function of radial coordinate r ,

$$z = -A \left(1 - \cos \frac{2\pi r}{\lambda} \right), \quad (1)$$

where A is the amplitude of the waviness and λ is its wavelength. In the analysis of Guduru (2007), only surfaces with positive values of A were considered, such that initial contact with the rigid sphere was made at a central convex asperity on the elastic wavy surface (i.e., the wavy surface has a peak at $r=0$). Here we will extend the analysis to include negative values of A , which will allow us to additionally consider axisymmetric wavy surfaces which have a central concave trough. The differences in the contact geometry between a sphere and two wavy surfaces with amplitudes of opposite sign are illustrated in Fig. 1.

As in the classical Hertz contact analysis, we approximate the rigid spherical surface as a paraboloid,

$$z = \frac{r^2}{2R}, \quad (2)$$

which is valid for small values of r/R , where R is the radius of the sphere. Thus, the gap between the sphere and the wavy surface is given by

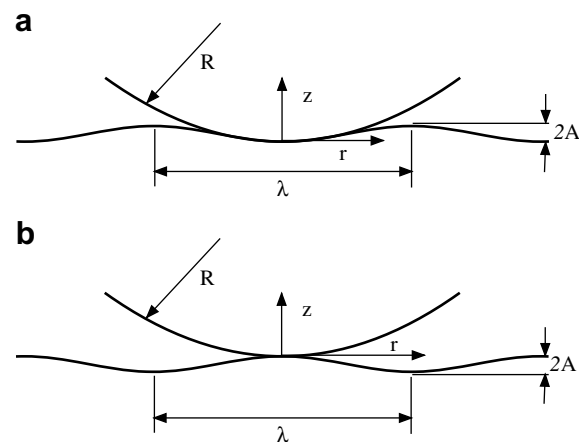


Fig. 1. The geometry of the axisymmetric contact problem. A sphere of radius R contacts an elastic half-space with a single wavelength cosine surface. The amplitude and wavelength have been exaggerated in the diagram for visual clarity. (a) $A < 0$, central concave trough. (b) $A > 0$, central convex asperity.

$$f(r) = \frac{r^2}{2R} + A \left(1 - \cos \frac{2\pi r}{\lambda} \right). \quad (3)$$

It is clear that as the rigid sphere is brought into contact, the contact area will not be simply connected for most wavy surface geometries. [Guduru \(2007\)](#) derived conditions for the gap given by Eq. (3) to be monotonically increasing with radius, which guarantees a simply connected contact area, but is overly restrictive as the presence of adhesion allows for a wavy surface to spontaneously achieve full contact in the absence of normal load, as shown by [Johnson \(1995\)](#) and others. Further, many soft elastomers such as polydimethylsiloxane (PDMS) allow for rapid air diffusion ([Hui et al., 2001](#)), such that it is possible for trapped air bubbles to disperse with time under external loading. For these reasons, we focus on the detachment problem of the sphere from the wavy surface, assuming that the sphere has been pressed sufficiently such that any partial contacts have coalesced and intimate contact is established throughout the contact area before detachment begins. We will further examine the conditions for spontaneous jump-to-contact in Section 2.6.

2.2. Sneddon theorems for axisymmetric contact problems

Following the procedure presented by [Maugis \(2000\)](#), we begin our study of the contact problem by reviewing helpful theorems derived by [Sneddon \(1965\)](#) for solving the axisymmetric indentation problem of a rigid punch of arbitrary profile in contact with a flat elastic half-space. For a given contact radius a , our wavy surface problem can be made equivalent to the flat surface formulation by making the profile of the rigid indenter, $f(\rho)$, equal to that of the gap given in Eq. (3), where $\rho = r/a$. In the solution procedure which follows, Δ is the penetration of the punch; P is the applied load ($P > 0$ indicating compression); $\sigma_z(r, 0)$ is the stress inside the area of contact; and $u_z(r, 0)$ is the displacement of surface points outside the area of contact. [Sneddon \(1965\)](#) showed that by defining the function

$$\chi(t) = \frac{2}{\pi} \left(\Delta - t \int_0^t \frac{f'(\rho) d\rho}{\sqrt{t^2 - \rho^2}} \right), \quad (4)$$

the contact parameters for an arbitrary punch profile $f(\rho)$ can be expressed as:

$$\Delta = \int_0^1 \frac{f'(x) dx}{\sqrt{1-x^2}} + \frac{\pi}{2} \chi(1) \quad (5)$$

$$P = \pi a E^* \int_0^1 \chi(t) dt = 2a E^* \left[\Delta - \int_0^1 \frac{x f(x)}{\sqrt{1-x^2}} dx \right] \quad (6)$$

$$\sigma_z(\rho, 0) = -\frac{E^*}{2a} \left[\frac{\chi(1)}{\sqrt{1-\rho^2}} - \int_\rho^1 \frac{\chi'(t) dt}{\sqrt{t^2 - \rho^2}} \right], \quad \rho < 1 \quad (7)$$

$$u_z(\rho, 0) = \int_0^1 \frac{\chi(t) dt}{\sqrt{\rho^2 - t^2}}, \quad \rho > 1 \quad (8)$$

Here, $E^* = E/(1-\nu^2)$ is the plane strain modulus of the elastic solid, which is characterized by the elastic modulus E and the Poisson's ratio ν . Physically, the function $\chi(t)$ determines the nature of the stresses at the periphery of contact. For Hertzian contact, the requirement that no stress singularity be present at $\rho = 1$ is enforced by prescribing $\chi(1) = 0$, and this condition determines the contact radius a . When adhesion is present, $\chi(1)$ can be non-zero ([Barquins and Maugis, 1982](#)), implying that singular contact stresses are admissible within the linear elasticity treatment of adhesion problems.

2.3. Hertzian contact of axisymmetric wavy surfaces

We begin the solution of the axisymmetric wavy contact problem by considering the Hertzian case where no adhesion is present. First we note that, from Eq. (3),

$$f'(\rho) = \frac{a^2 \rho}{R} + \frac{2\pi a A}{\lambda} \sin \frac{2\pi a \rho}{\lambda}, \quad (9)$$

and thus we can solve for $\chi(t)$ using Eq. (4):

$$\chi(t) = \frac{2}{\pi} \left[\Delta_1 - \frac{a^2 t^2}{R} - \frac{\pi^2 A a t}{\lambda} H_0 \left(\frac{2\pi a t}{\lambda} \right) \right], \quad (10)$$

where Δ_1 is the penetration in the absence of adhesion and $H_n(\cdot)$ is the Struve function of order n (c.f. [Abramowitz and Stegun, 1965](#)). To ensure nonsingular stresses at the periphery of contact we require $\chi(1) = 0$, and using this condition to solve Eq. (10) for Δ_1 , we find

$$\Delta_1 = \frac{a^2}{R} + \frac{\pi^2 A a}{\lambda} H_0 \left(\frac{2\pi a}{\lambda} \right). \quad (11)$$

Substituting this expression into Eq. (10) and using Eq. (8) to solve for the Hertzian displacement $u_{z,1}$, we find:

$$u_{z,1}(\rho) = \frac{a^2}{\pi R} \left[(2 - \rho^2) \sin^{-1} \frac{1}{\rho} + \sqrt{\rho^2 - 1} \right] + \frac{2\pi A a}{\lambda} \left[H_0 \left(\frac{2\pi a}{\lambda} \right) \sin^{-1} \frac{1}{\rho} - \int_0^1 \frac{t H_0(2\pi a t / \lambda)}{\sqrt{\rho^2 - t^2}} dt \right]. \quad (12)$$

Using Eq. (7) to solve for the contact pressure, $p_1(r) = -\sigma_z(r, 0)$, for a given radius a in the absence of adhesion results in the expression

$$p_1(r) = \frac{E^*}{\pi} \left[\left(\frac{2}{R} + \frac{4\pi^2 A}{\lambda^2} \right) \sqrt{\alpha^2 - r^2} + \frac{\pi^2 A}{\lambda} \int_r^a \frac{H_0(2\pi \alpha / \lambda)}{\sqrt{\alpha^2 - r^2}} d\alpha - \frac{2\pi^3 A}{\lambda^2} \int_r^a \frac{H_1(2\pi \alpha / \lambda)}{\sqrt{\alpha^2 - r^2}} d\alpha \right]. \quad (13)$$

Finally, the total applied load can be found by using Eq. (6):

$$P_1(r) = 2E^* \left[\left(\frac{2}{R} + \frac{4\pi^2 A}{\lambda^2} \right) \frac{a^3}{3} + \frac{\pi A a}{2} H_1 \left(\frac{2\pi a}{\lambda} \right) - \frac{\pi^2 A a^2}{\lambda} H_2 \left(\frac{2\pi a}{\lambda} \right) \right]. \quad (14)$$

Note that although [Guduru \(2007\)](#) used a different solution procedure (the method of cumulative superposition, e.g. [Hill and Storakers \(1990\)](#)), the results of both solution techniques for p_1 , P_1 , and Δ_1 are identical. The Sneddon procedure is better suited for our current purposes in that it gives a simple formula for obtaining u_z , which is necessary later for studying the influence of adhesive tractions outside the contact area.

2.4. JKR adhesive contact of axisymmetric wavy surfaces

As demonstrated by [Guduru \(2007\)](#), the adhesion problem between the rigid sphere and the wavy surface can be solved in several ways. In the JKR model of two adhering surfaces, it is assumed that adhesive forces only act within the area of contact and that the interaction between the surfaces outside the contact area is negligible. Either the original JKR potential energy approach ([Johnson et al., 1971](#)) or the equivalent energy release rate approach of linear elastic fracture mechanics ([Maugis, 2000](#)) can be used. In both cases, the final adhered state can be obtained by superposing the Hertzian wavy surface contact solution presented above, for a given contact radius a and load P_1 in the absence of adhesion given by Eq. (14), and the solution for a rigid circular punch of the same radius a on a half-space with an applied load of $P_1 - P$, where P is the applied load required to maintain the contact radius a on the wavy surface in the presence of adhesion. The contact pressure resulting from such a superposition is

$$p(r) = p_1(r) - \frac{P_1 - P}{2\pi a^2 \sqrt{1 - r^2/a^2}}, \quad (15)$$

where $p_1(r)$ is given by Eq. (13). The mode I stress intensity factor at the contact boundary is defined as

$$K_I = \lim_{r \rightarrow a} \sqrt{2\pi(a-r)p(r)} = \frac{P_1 - P}{2a\sqrt{\pi a}}, \quad (16)$$

and the corresponding energy release rate can be evaluated as

$$G = \frac{K_I^2}{2E^*} = \frac{(P_1 - P)^2}{8\pi E^* a^3}. \quad (17)$$

(The energy release rate is half that in fracture mechanics because the punch is not deformable). At equilibrium, the energy release rate G is equal to the work of adhesion,

$$w = \Delta\gamma = \gamma_1 + \gamma_2 - \gamma_{12}, \quad (18)$$

where γ_1 and γ_2 are the surface energies of the contacting solids and γ_{12} is interaction energy between the two materials. Thus, the equilibrium condition $G = w$ determines the JKR solution for the applied load, from Eq. (17), to be

$$P(a) = P_1(a) - \sqrt{8\pi E^* w a^3}. \quad (19)$$

Similarly, the JKR penetration and displacement can be obtained by superposing the flat punch results (Maugis, 2000):

$$\Delta = \Delta_1 - \frac{\sqrt{\pi a}}{E^*} K_I = \Delta_1 - \sqrt{\frac{2\pi w a}{E^*}} \quad (20)$$

$$u_z(\rho, 0) = u_{z,1}(\rho, 0) - \frac{2}{\pi E^*} K_I \sqrt{\pi a} \sin^{-1} \frac{1}{\rho}, \quad \rho > 1 \quad (21)$$

Hence, for a given contact radius a , the corresponding load P and penetration Δ can be represented in a parametric plot using Eqs. (19) and (20). Guduru (2007) has investigated the JKR adhesion model for axisymmetric surfaces in detail. Here, we proceed to introduce new dimensionless parameters which permit a comprehensive mapping of the Guduru (2007) results.

2.5. Dimensionless JKR theory for axisymmetric wavy surface contact

The JKR theory presented above can be represented in dimensionless form with the introduction of the following parameters:

$$\alpha = \frac{AR}{\lambda^2}, \quad \beta = \left(\frac{\lambda}{R}\right)^3 \frac{E^* R}{2\pi w} = \frac{\lambda^3 E^*}{2\pi w R^2} \quad (22)$$

Physically, α represents the degree of surface waviness. Larger values of α correspond to surfaces with high amplitude, short wavelength waviness, whereas smaller values of α correspond to surfaces with shallow, long wavelength waviness. β is a measure of the relative stiffness of the material to the surface energy; small β values correspond to more compliant materials where surface energy effects are more dominant, whereas large β values correspond to stiffer materials where surface energy is less dominant. Using these parameters, and defining the normalized load, penetration, and contact radius as

$$\bar{P} = \frac{P}{\pi w R}, \quad \bar{\Delta} = \frac{\Delta R}{\lambda^2}, \quad \bar{a} = \frac{a}{\lambda}, \quad (23)$$

respectively, dimensionless expressions for the Hertzian contact load \bar{P}_1 , JKR contact load \bar{P} , and JKR penetration $\bar{\Delta}$ are obtained from Eqs. (14), (19), and (20):

$$\bar{P}_1 = 4\beta \left[\frac{2\bar{a}}{3} + \alpha \left(\frac{4\pi^2 \bar{a}^3}{3} + \frac{\pi \bar{a}}{2} H_1(2\pi \bar{a}) - \bar{a}^2 H_2(2\pi \bar{a}) \right) \right] \quad (24)$$

$$\bar{P} = \bar{P}_1 - 4\sqrt{\beta \bar{a}^3} \quad (25)$$

$$\bar{\Delta} = \bar{a}^2 + \alpha \pi^2 \bar{a} H_0(2\pi \bar{a}) - \sqrt{\frac{\bar{a}}{\beta}} \quad (26)$$

As $\alpha \rightarrow 0$, the solution for JKR adhesion of a rigid sphere on a flat elastic surface is recovered.

Graphs of the load \bar{P} versus the penetration $\bar{\Delta}$ illustrate how the presence of surface waviness introduces oscillations onto the equilibrium load curves, as seen in Fig. 2. Here, the dashed line represents the equilibrium path for this particular combination of α and β . However, during detachment, the equilibrium path cannot be followed, and there will be unstable jumps to the next physically achievable point on the curve, shown by the solid arrows which follow the detachment path for the case of displacement-controlled separation. Such instabilities dissipate energy, illustrated by the shaded portion of the graph, and cause toughening of the contact interface. This phenomenon of energy dissipation is not captured by other existing models of rough or wavy surface adhesion, and indicates that models which assume that the contact approach and separation are perfectly reversible processes are neglecting a fundamental mechanism for interface toughening.

The separation or pull-off force, \bar{P}_c , is the maximum tensile load supported during detachment. In a load-controlled experiment, the two surfaces will spontaneously separate once \bar{P}_c is reached. With the sign convention adopted here, the maximum tensile load corresponds to the minimum point on the \bar{P} - $\bar{\Delta}$ curves. From the classical JKR analysis for a rigid sphere detaching from a flat elastic surface, $(\bar{P}_c)_{\text{flat}} = -\frac{3}{2}$. The location of \bar{P}_c on the \bar{P} - $\bar{\Delta}$ curves is illustrated in Fig. 3.

2.6. Discussion

The results of Section 2.5 allow for comprehensive plots of the pull-off force enhancement $\bar{P}_c = (\bar{P}_c)_{\text{wavy}}/(\bar{P}_c)_{\text{flat}}$ using only the parameters α and β . Such a map of the predicted adhesion enhancement for a range of wavy surfaces is presented in Fig. 4. A significant enhancement in the normalized pull-off force is seen for the majority of combinations of α and β , including both $\alpha > 0$ (central convex asperity) and $\alpha < 0$ (central concave trough). The general trend is that the force amplification \bar{P}_c tends to increase as β increases, although there are some combinations of α and β for which $\bar{P}_c < 1$, meaning that the pull-off force for the wavy surface characterized by those parameters is less than that for the flat surface. However, significant enhancement in adherence is clearly attainable for most geometries. The adhesion map in Fig. 4 shows that fivefold increase in pull-off force is predicted for several combinations of $|\alpha| < 0.5$, $1 \leq \beta \leq 10$. Even greater increases in pull-off force are predicted by this model for higher values of α , β . The experimental work of Guduru and Bull (2007) showed that

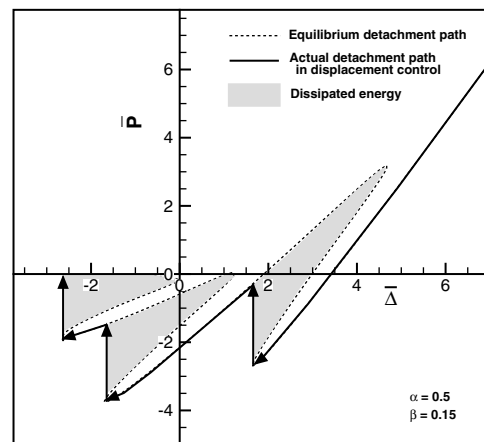


Fig. 2. Variation of the compressive normal load \bar{P} as a function of the penetration $\bar{\Delta}$, for JKR adhesion. Energy dissipation (shaded areas) due to unstable detachment results in interface toughening.

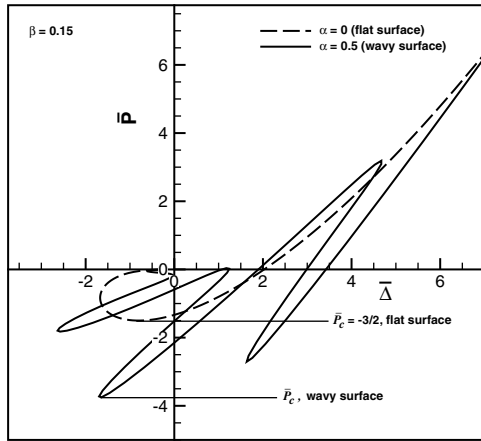


Fig. 3. The minimum point on the load–penetration curve corresponds to the pull-off force \bar{P}_c , and is generally larger in magnitude for the wavy geometry than the pull-off force for the sphere on a flat surface, resulting in interface strengthening.

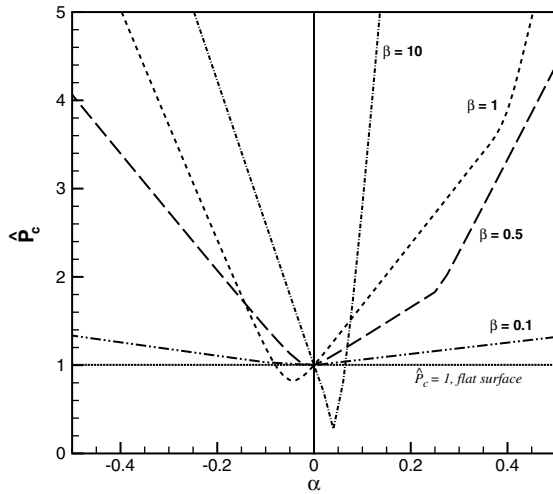


Fig. 4. Map of pull-off force amplification factor for the wavy surface, \bar{P}_c , predicted by the JKR adhesion analysis for various dimensionless parameters $\alpha = \frac{AR}{\lambda^2}$, $\beta = \frac{\lambda^3 E^*}{2\pi w R^2}$.

$5 \leq \bar{P}_c \leq 15$ was easily attainable for rigid wavy surfaces separating from soft gelatin, with $0.25 \leq \alpha \leq 1.25$ and $0.2 \leq \beta \leq 20$. Using the data from Fig. 4 for the specific case of PDMS, with typical modulus $E^* \approx 1$ MPa and work of adhesion $w \approx 50$ mJ/m², in contact with a rigid sphere of radius 5 mm, choosing $\alpha = 0.15$ and $\beta = 1$ results in pull-off force amplification $\bar{P}_c \approx 2$, and corresponds to waviness amplitude $A = 1.2$ μ m and wavelength $\lambda = 0.2$ mm. Choosing $\alpha = 0.15$ and $\beta = 10$ results in pull-off force amplification $\bar{P}_c \approx 6$, and corresponds to waviness amplitude $A = 5.5$ μ m and wavelength $\lambda = 0.43$ mm. These examples illustrate the potential for significant increases in adhesive tenacity resulting from the presence of shallow waviness on soft elastic surfaces.

In the construction of Fig. 4, it is assumed that full intimate contact has been reached within a sufficiently large radius \bar{a} such that the maximum pull-off force predicted by the \bar{P} – $\bar{\Delta}$ curves can be achieved in the detachment problem. To better understand the conditions for the validity of such an assumption, we can qualitatively study the conditions for spontaneous jump-to-contact during approach using the Persson global energy balance concept (e.g. Persson, 2002). First, we estimate the energy necessary to deform an elastic block so that the material fills a substrate cavity of height A and width λ :

$$U_{el} \approx \frac{1}{2} \int_V \sigma \epsilon d^3x, \quad (27)$$

where the stress $\sigma \approx E\epsilon$, and the strain $\epsilon \approx A/\lambda$ is mainly localized to a volume $\approx \lambda^3$. Hence, an approximation for the elastic energy is $U_{el} \approx \lambda^3 E \left(\frac{A}{\lambda}\right)^2 = EA^2$. The gain in the adhesion energy upon contact is $U_{ad} \approx -w \lambda^2$. Setting $U_{el} = -U_{ad}$ gives

$$\frac{A}{\lambda} \approx \left(\frac{w}{E\lambda}\right)^{1/2}. \quad (28)$$

Making the approximation $E \approx E^*$ for the purposes of this qualitative analysis, and dividing both sides by λ/R , Eq. (28) can be rewritten as

$$\alpha \approx \left(\frac{1}{2\pi\beta}\right)^{1/2}. \quad (29)$$

Thus, the surfaces will spontaneously jump to contact in the absence of applied load if $\alpha \leq \alpha_c \approx (2\pi\beta)^{-1/2}$. Combinations of α and β where this condition is met is illustrated within the shaded area in Fig. 5. For geometries where $\alpha > \alpha_c$, the curves for the amplification in pull-off force \bar{P}_c seen during detachment are only valid after full contact has first been obtained by external compressive loading.

In Fig. 5, it can be seen that beyond a critical β , there is actually a reduction in pull-off force for the wavy surface compared to the flat surface, i.e., $\bar{P}_c < 1$. (As noted previously, this effect is also seen in Fig. 4). This corresponds to the case where locally the wavelength becomes large enough that the contact problem becomes one of two isolated spherical asperities in contact, rather than a wavy surface. In such a case, the effective radius is smaller than the radius R , and thus the apparent pull-off force decreases, so that $\bar{P}_c < 1$.

Thus far, the analysis only allows for interface separation originating at the periphery. However, intuitively it can be seen that above a critical amplitude of waviness, interface separation is likely to occur at the local minima of the surface waves, where tensile interface stresses will be highest. Other authors (e.g. Johnson, 1995) have allowed for this possibility by seeding these local minima with small flaws, since introducing local imperfections is the only way to initiate crack growth along a perfect interface in the Griffith model of fracture mechanics. Unlike the case of the planar wavy surface model studied by Johnson (1995), the local minima for the axisymmetric gap profile of Eq. (3) are not radially periodic or ordered for general α and β , and this significantly complicates such an analysis. Therefore, while considering the case of crack ini-

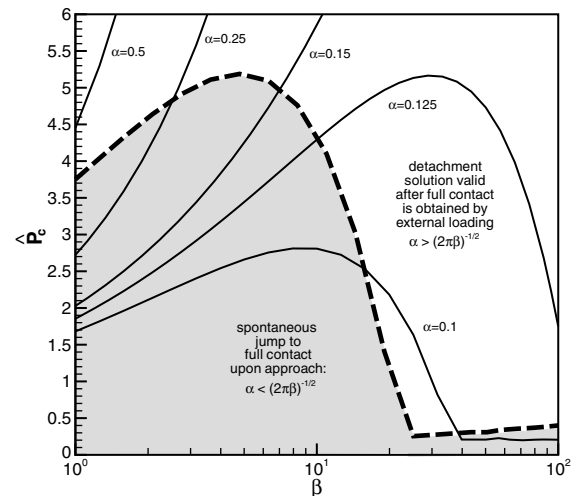


Fig. 5. Adhesion amplification map illustrating the regions where spontaneous jump to full contact upon approach is possible for a selected range of α , β .

tiation at interface flaws is necessary to fully complete the wavy surface adhesion model, we will not consider it in the current dimensionless analysis and simply note that in practice, for given values of λ and R there is a critical value of A beyond which interface separation will initiate within the contact region, and this will significantly reduce any adherence of the two solids, as typically seen for rough surfaces.

3. Axisymmetric wavy surface adhesion: JKR–DMT transition

3.1. Background on major theories of adhesion

The analytical formulation presented above is based on the JKR (Johnson et al., 1971) theory, in which the key assumption is the absence of surface interactions between the sphere and the wavy surface outside the area of intimate contact. Such a model is well-suited for modeling soft, compliant materials with high surface energy. However, attractive forces outside the edge of contact become more important for stiffer materials with low surface energy which do not deform as significantly when placed into contact. These conditions are better captured by the DMT (Derjaguin et al., 1975) model, which assumes that molecular forces act only in a ring-shaped zone of noncontact adhesion, and are assumed not to change the shape of the profile outside the contact area from the Hertzian solution (as the materials are stiff). Muller et al. (1983) later presented a revised DMT model, using a more correct method to sum up the interactions in the Hertzian gap. Note that while $(\bar{P}_c)_{\text{flat}} = -\frac{3}{2}$ for the JKR model, $(\bar{P}_c)_{\text{flat}} = -2$ for the DMT model.

Tabor (1977) compared the two theories and showed they were related by a dimensionless transition parameter μ which evaluates the ratio of elastic deformation to the range of the surface forces. Muller et al. (1980) implemented a numerical Lennard–Jones surface interaction potential and confirmed a continuous transition between the DMT and JKR regimes, governed by a parameter proportional to Tabor's adhesive transition parameter. The DMT regime corresponds to $\mu \ll 1$, for stiff materials, small spherical indenter radius R , and low surface energy w . The JKR regime corresponds to $\mu \gg 1$, for compliant materials, large R , and high w . (In their adhesion map for the contact of elastic spheres, Johnson and Greenwood (1997) show that the JKR theory is strictly valid for $\mu > 5$ but that it works well for $\mu > 0.3$ in practice.)

For contact problems in the transition region between the two adhesion theories, Maugis (1992) introduced a solution based on a Dugdale (1960) model for the surface interactions rather than the more realistic Lennard–Jones model, which makes the problem tractable analytically. In the Dugdale assumption for the interaction potential, the adhesive traction is constant at a value of σ_0 until the critical crack opening separation δ_c is reached, and the adhesive stress immediately drops to zero for larger separations. Although this is an approximation to the actual adhesive interaction, Barthel (1998) showed that the Dugdale model is adequate in most cases. The transition parameter used by Maugis is commonly referred to as λ , but will be called μ_m here to avoid confusion with the wavelength of surface waviness, and is defined as

$$\mu_m = \frac{\sigma_0}{E^*} \left(\frac{9RE^*}{2\pi w} \right)^{1/3}. \quad (30)$$

If the Dugdale adhesive traction σ_0 is chosen to match the maximum adhesive traction given by the Lennard–Jones interaction potential, then it has been demonstrated that $\mu_m = 1.16 \mu$ (Johnson and Greenwood, 1997). In the derivation that follows, we extend the Maugis–Dugdale transition model to the axisymmetric wavy surface adhesive contact problem.

3.2. Maugis–Dugdale cohesive zone model for axisymmetric wavy surfaces

In the Maugis–Dugdale model for axisymmetric problems (Maugis, 1992, 2000), the adhesive stress is assumed to reach a constant tensile value σ_0 on an annulus outside the contact zone. At the outer edge of this annulus, a critical separation δ_c between the two contacting surfaces is reached, and the adhesive stress drops to zero, as illustrated in Fig. 6a. The size of this annular cohesive zone is determined such that the stress singularity at the edge of the contact area in the JKR model is canceled, so that the crack profile closes smoothly without a discontinuity in slope. The condition governing the cancellation of stress singularities can be expressed as

$$K_I + K_m = 0, \quad (31)$$

where K_I is the stress intensity factor found from the JKR analysis due to the external loading, and K_m is the stress intensity factor resulting from the introduction of the tensile adhesive tractions at the contact periphery. Recall from Eq. (15) that the singular contact stress in the JKR adhesion problem is defined as

$$\sigma_z(r, 0) = \frac{K_I}{\sqrt{\pi a}} \frac{1}{\sqrt{1 - \rho^2}} - p_1(r), \quad (32)$$

where K_I is defined by Eq. (16). The stress distribution due to constant adhesive traction σ_0 on an annulus ($a < r < c$) is given by Maugis (2000) as

$$\sigma_z(r, 0) = \frac{K_m}{\sqrt{\pi a}} \frac{1}{\sqrt{1 - \rho^2}} + \frac{2\sigma_0}{\pi} \tan^{-1} \sqrt{\frac{m^2 - 1}{1 - \rho^2}} \quad (33)$$

where the stress intensity factor from the presence of the cohesive zone is

$$K_m = -\frac{\sigma_0 a}{\sqrt{\pi a}} \left[\sqrt{m^2 - 1} + m^2 \tan^{-1} \sqrt{m^2 - 1} \right] \quad (34)$$

and the parameter $m = c/a$ defines the size of the cohesive zone outside the contact area, as shown in Fig. 6b. Thus, substituting Eqs. (16) and (34) into Eq. (31) and solving for the external load for the contact problem in the presence of Dugdale cohesive zones, P_m , we find

$$P_m = P_1 - 2\sigma_0 a^2 \left[\sqrt{m^2 - 1} + m^2 \tan^{-1} \sqrt{m^2 - 1} \right]. \quad (35)$$

The contact stresses are additive:

$$\sigma_{z,m}(r, 0) = -p_1(r) + \frac{2\sigma_0}{\pi} \tan^{-1} \sqrt{\frac{m^2 - 1}{1 - \rho^2}}. \quad (36)$$

Hence the outcome of the stress analysis is the relationship between load P_m and contact radius a in terms of the cohesive strength σ_0 and cohesive zone size m . The penetration Δ_m for the Maugis–Dugdale model is given by Maugis (2000) as the sum of Δ , the JKR penetration, and the approach due to the adhesive forces outside the contact:

$$\Delta_m = \Delta + \frac{\sigma_0 a}{E^*} \left[m^2 \tan^{-1} \sqrt{m^2 - 1} - \sqrt{m^2 - 1} \right]. \quad (37)$$

Substituting for Δ from Eq. (20) and using $K_I = -K_m$, as defined by Eqs. (31) and (34), the penetration Δ_m is found to be

$$\Delta_m = \frac{a^2}{R} + \frac{\pi^2 A a}{\lambda} H_0 \left(\frac{2\pi a}{\lambda} \right) - \frac{2\sigma_0 a}{E^*} \sqrt{m^2 - 1}. \quad (38)$$

In order to use these equations, we must solve for the cohesive zone size m . The equilibrium energy release rate G at the crack tip, which is simply $G = w = \sigma_0 \delta_c$ in the Dugdale model, determines the value of m for a given value of contact radius a . In order to proceed, we need an expression for the crack opening displacement δ_c , which is the gap $[u_z]$ between the rigid punch and the deformed surface at the

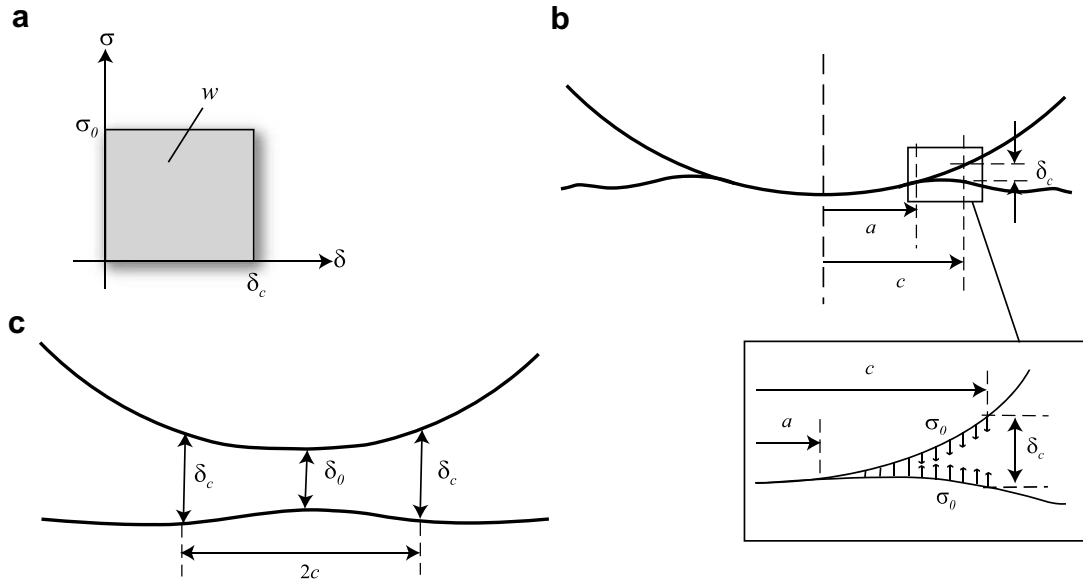


Fig. 6. Illustrations of the assumptions of the Maugis–Dugdale model for the JKR–DMT transition. (a) Dugdale model for adhesion outside the area of intimate contact, with constant adhesive traction σ_0 acting over a cohesive zone length δ_c . (b) Schematic of the contact radius a and cohesive zone $a \leq r \leq c$, where adhesive surface interactions are present. (c) Schematic of the cohesive zone $r \leq c$ for the noncontact case, $a = 0$.

end of the cohesive zone, $r = c$. The gap $[u_z]$ can be obtained once the displacement profile $u_z(r, 0)$ is determined, as shown in Fig. 7:

$$\delta_c = [u_z(c)] = f(c) - \Delta + u_z(c, 0), \quad (39)$$

where Δ is the penetration of the punch and the shape function $f(r)$ is given by Eq. (3). To find $[u_z(\rho, 0)]$ in the presence of cohesive stresses, we follow the procedure of Maugis (2000) by first substituting Eqs. (3) and (20,21) into Eq. (39) to express the gap for the JKR problem:

$$\begin{aligned} [u_z(\rho, 0)]_{\text{JKR}} = & \frac{2}{\pi E^*} K_I \sqrt{\pi a} \cos^{-1} \frac{1}{\rho} + \frac{a^2}{\pi R} \left[\sqrt{\rho^2 - 1} - (2 - \rho^2) \cos^{-1} \frac{1}{\rho} \right] \\ & + A \left[1 - \cos \frac{2\pi a \rho}{\lambda} - \frac{\pi^2 a}{\lambda} H_0 \left(\frac{2\pi a}{\lambda} \right) \right. \\ & \left. + \frac{2\pi a}{\lambda} H_0 \left(\frac{2\pi a}{\lambda} \right) \sin^{-1} \frac{1}{\rho} - \frac{2\pi a}{\lambda} \int_0^1 \frac{t H_0(2\pi a t / \lambda)}{\sqrt{\rho^2 - t^2}} dt \right] \end{aligned} \quad (40)$$

Then we must account for the reduction in the gap $[u_z]$ due to the presence of the tensile traction σ_0 acting outside the contact area within the Dugdale cohesive zone. From Maugis (2000), this change in displacement is:

$$\begin{aligned} u_T(\rho) = & -\frac{4\sigma_0 a}{\pi E^*} \left[\sqrt{m^2 - 1} \left(\sqrt{\rho^2 - 1} - \cos^{-1} \frac{1}{\rho} \right) - m^2 \int_1^{\min(\rho, m)} \frac{\sqrt{\rho^2 - t^2}}{t^2 \sqrt{m^2 - t^2}} dt \right] \\ & + \frac{2K_m}{\pi E^*} \sqrt{\pi a} \cos^{-1} \frac{1}{\rho} \end{aligned} \quad (41)$$

Adding u_T to $[u_z]_{\text{JKR}}$ and recalling that $K_I + K_m = 0$, we can express the crack opening $\delta_c = [u_z(m)]$ at the edge of the cohesive zone ($\rho = m$) as:

$$\begin{aligned} \delta_c = & \frac{a^2}{\pi R} \left[\sqrt{m^2 - 1} + (m^2 - 2) \tan^{-1} \sqrt{m^2 - 1} \right] \\ & + \frac{4\sigma_0 a}{\pi E^*} \left[\sqrt{m^2 - 1} \tan^{-1} \sqrt{m^2 - 1} - m + 1 \right] \\ & + A \left[1 - \cos \frac{2\pi a m}{\lambda} - \frac{\pi^2 a}{\lambda} H_0 \left(\frac{2\pi a}{\lambda} \right) + \frac{2\pi a}{\lambda} H_0 \left(\frac{2\pi a}{\lambda} \right) \sin^{-1} \frac{1}{m} \right. \\ & \left. - \frac{2\pi a}{\lambda} \int_0^1 \frac{t H_0(2\pi a t / \lambda)}{\sqrt{m^2 - t^2}} dt \right] \end{aligned} \quad (42)$$

Here, the identity $\cos^{-1}(1/x) = \tan^{-1} \sqrt{x^2 - 1}$ if $x > 0$ has been used to simplify the expression. Recall that $G = \sigma_0 \delta_c = w$ at onset of crack initiation. By multiplying the expression for δ_c by σ_0 and equating this to w , we obtain an expression to solve for cohesive zone size m . (Solving for m must be done numerically as a closed form analytical solution for m does not exist).

3.3. Noncontact cohesive zone solution

The above Maugis solution procedure assumes the presence of a region of intimate contact within the radius $a > 0$. Kim et al. (1998) presented an important extension of the Maugis solution for the case where the surfaces are not within intimate contact ($a = 0$) but are within the range of adhesive interaction ($c > 0$). Such a case is illustrated in Fig. 6c. Following Kim's procedure, the gap between the surfaces at $r = c$ in this “noncontact” regime is defined as

$$\delta_c - u_z(r = c) = \delta_0 - u_z(r = 0) + \frac{c^2}{2R} + A \left(1 - \cos \frac{2\pi c}{\lambda} \right), \quad (43)$$

where the surface displacement due to the presence of the adhesive tractions is approximated by the solution for the vertical displacement of a half-space under constant stress σ_0 within a radius c (Johnson, 1985):

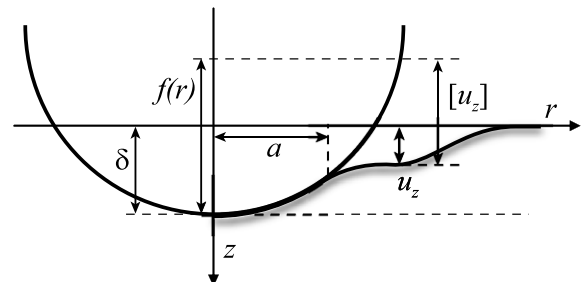


Fig. 7. Illustration of the gap $[u_z]$ between the rigid sphere and the deformed surface, outside the area of contact.

$$u_z(r=0) = -\frac{2\sigma_0 c}{E^*} \quad (44)$$

$$u_z(r=c) = -\frac{4\sigma_0 c}{\pi E^*} \quad (45)$$

Defining $\xi = \delta_0/\delta_c$, and noting that $\delta_c = w/\sigma_0$, Eq. (43) yields

$$\xi + \frac{2\sigma_0^2 c(\pi-2)}{\pi E^* w} + \frac{c^2}{2R} \frac{\sigma_0}{w} + A \frac{\sigma_0}{w} \left(1 - \cos \frac{2\pi c}{\lambda}\right) = 1. \quad (46)$$

For a given $\xi \leq 1$, Eq. (46) can be solved numerically for c . In doing so, we implicitly assume that the gap within the region of noncontact adhesion increases monotonically with radius, such that the gap at $r=c$ is always larger than the gap at all $r < c$. This assumption will only be valid for the case of $\alpha > 0$ where the slope of the separation gap $f(r) > 0$. Guduru (2007) noted that these conditions are met when $\alpha < 0.117$. Hence, the results of this noncontact analysis are only valid for such conditions.

Once c is known, the normal load is found by integrating the cohesive traction within the adhesive contact radius,

$$P = -\sigma_0 \pi c^2, \quad (47)$$

and the normal approach is defined as

$$\Delta = -\delta_0 + u_z(r=0) = -\delta_0 - \frac{2\sigma_0 c}{E^*}. \quad (48)$$

Eqs. (46)–(48) completely define the contact problem for the Kim et al. (1998) model of the noncontact regime. In a recent paper, Shi and Polycarpou (2005) demonstrated that the assumption of a constant cohesive traction σ_0 in the Kim model tends to overestimate the adhesive stress under noncontacting conditions and artificially limits the effective separation range of adhesive stress, δ_c , to a very small value. Although the noncontact model proposed by Shi and Polycarpou is more physically accurate than the model described here, we are primarily interested in the detachment problem for wavy surface contact rather than the approach problem so the less numerically-intensive Kim model described above is adequate.

3.4. Dimensionless theory for the Maugis–Dugdale wavy surface contact problem

The Maugis transition solution presented above can be summarized using dimensionless parameters as follows. In the contact regime where $a > 0$, writing $\sigma_0 \delta_c = w$, and simplifying the above expressions using α , β , and the following definition for μ_m ,

$$\mu_m = \frac{\sigma_0}{E^*} \left(\frac{9RE^*}{2\pi w} \right)^{1/3} = \frac{\sigma_0}{E^*} \frac{R}{\lambda} (9\beta)^{1/3}, \quad (49)$$

we find that the governing equation for the cohesive zone size m can be written as

$$\begin{aligned} 1 = & 2\mu_m \bar{a}^2 \left(\frac{\beta}{3} \right)^{2/3} \left[\sqrt{m^2 - 1} + (m^2 - 2) \tan^{-1} \sqrt{m^2 - 1} \right] \\ & + \frac{8}{3} \mu_m^2 \bar{a} \left(\frac{\beta}{3} \right)^{1/3} \left[\sqrt{m^2 - 1} \tan^{-1} \sqrt{m^2 - 1} - m + 1 \right] \\ & + 2\pi\mu_m \alpha \left(\frac{\beta}{3} \right)^{2/3} \left[1 - \cos 2\pi \bar{a} m - \pi^2 \bar{a} H_0(2\pi \bar{a}) \right. \\ & \left. + 2\pi \bar{a} H_0(2\pi \bar{a}) \sin^{-1} \frac{1}{m} - 2\pi \bar{a} \int_0^1 \frac{t H_0(2\pi \bar{a} t)}{\sqrt{m^2 - t^2}} dt \right] \end{aligned}$$

and the dimensionless normal load and approach can be expressed as

$$\bar{P}_m(\bar{a}) = \bar{P}_1(\bar{a}) - 4\mu_m \bar{a}^2 \left(\frac{\beta}{3} \right)^{2/3} \left[\sqrt{m^2 - 1} + m^2 \tan^{-1} \sqrt{m^2 - 1} \right], \quad (51)$$

$$\bar{\Delta}_m = \bar{a}^2 + \bar{a} \left[\pi^2 \alpha H_0(2\pi \bar{a}) - 2\mu_m \left(\frac{1}{9\beta} \right)^{1/3} \sqrt{m^2 - 1} \right]. \quad (52)$$

Also, the contact stress for the case $a > 0$, $\rho < 1$ can be expressed as

$$\begin{aligned} \frac{\sigma_z(\rho, 0)}{\sigma_0} \mu_m = & (9\beta)^{1/3} \left\{ \bar{a} \left[2\pi \alpha \int_\rho^1 \frac{\xi H_1(2\pi \bar{a} \xi)}{\sqrt{\xi^2 - \rho^2}} d\xi \right. \right. \\ & \left. \left. - \left(\frac{2}{\pi} + 4\pi \alpha \right) \sqrt{1 - \rho^2} \right] - \pi \alpha \int_\rho^1 \frac{H_0(2\pi \bar{a} \xi)}{\sqrt{\xi^2 - \rho^2}} d\xi \right\} \\ & + \frac{2}{\pi} \mu_m \tan^{-1} \sqrt{\frac{m^2 - 1}{1 - \rho^2}}. \end{aligned} \quad (53)$$

Similarly, the equation for the cohesive zone size $\bar{c} = c/\lambda$ in the non-contact regime can be expressed as

$$\xi + \frac{4}{3} (\pi - 2) \mu_m^2 \bar{c} \left(\frac{\beta}{3} \right)^{1/3} + \pi \mu_m \left(\frac{\beta}{3} \right)^{2/3} [\bar{c}^2 + 2\alpha(1 - \cos 2\pi \bar{c})] = 1, \quad (54)$$

and the dimensionless normal load and approach are found to be

$$\bar{P} = -2\pi \bar{c}^2 \mu_m \left(\frac{\beta}{3} \right)^{2/3}, \quad (55)$$

$$\bar{\Delta} = -\frac{\xi}{2\pi \mu_m} \left(\frac{3}{\beta} \right)^{2/3} - \frac{2\bar{c} \mu_m}{3} \left(\frac{3}{\beta} \right)^{1/3}. \quad (56)$$

Eqs. (50)–(52) and (54)–(56) fully describe the Maugis–Dugdale contact problem for wavy surface adhesion. Just as for the case of JKR adhesion, plots of load \bar{P}_m versus normal approach $\bar{\Delta}_m$ can be obtained. Fig. 8 shows a representative $\bar{P}_m, \bar{\Delta}_m$ plot for a range of μ_m for the case $\alpha = 0.1$, $\beta = 1$. For $\mu_m \rightarrow 0$, the wavy surface pull-off force (the minimum point on the load curve) $\bar{P}_c \rightarrow -2$, the same limiting pull-off force seen the DMT regime for a flat surface. As μ_m increases, $|\bar{P}_c|$ is seen to decrease slightly, and then increases again as μ_m begins to approach the JKR limit (solid line). Similar trends are seen for the case of $\alpha = 0.1, \beta = 10$, where there is a much more significant increase in pull-off force in the JKR regime, as seen in Fig. 9. Enhancement in adhesion is not seen for low values of μ_m near the DMT regime, which seems to be a general trend, as discussed below.

Using the dimensionless Maugis–Dugdale transition results, we can construct an adhesion map of the wavy surface pull-off force \bar{P}_c for a range of μ_m , similar to the adhesion map shown by Johnson and Greenwood (1997) for a sphere detaching from a flat surface. Such a map is shown for $0 \leq \alpha \leq 0.1$ in Fig. 10 ($\beta = 1$) and Fig. 11 ($\beta = 10$), where the $\alpha = 0$ curve corresponds to the Johnson–Greenwood solution. It is seen that adhesion enhancement (as evidenced by $|\bar{P}_c|$ increasing) is not present for values of μ_m approaching the

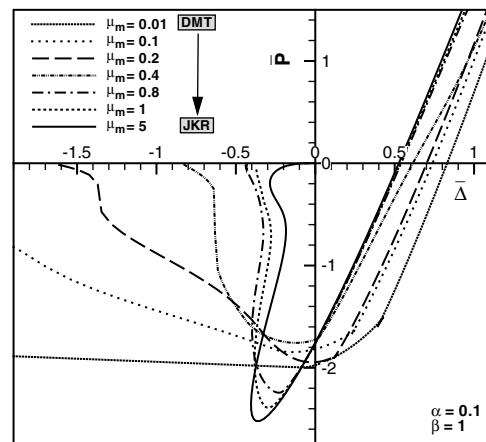


Fig. 8. Representative plot of normal load \bar{P} versus $\bar{\Delta}$ for the Maugis–Dugdale wavy surface adhesion problem, for a range of μ_m within the JKR–DMT transition regime. $\beta = 1$.

DMT regime. As μ_m increases, however, there is a clear transition point ($\mu_m \approx 0.4$ for these particular combinations of α, β) beyond which adhesion enhancement is evident. The magnitude of the adhesion enhancement increases with increasing α .

To understand why adhesion enhancement is not seen in the DMT regime, recall that the main assumptions of the DMT adhesion theory are that the elastic material is stiff and does not deform significantly when brought into contact; the molecular forces act only in a ring-shaped zone of noncontact adhesion; and these forces are assumed not to change the displacement outside the contact region from the Hertzian solution. Essentially, in the DMT regime the wavy surface is too rigid for the adhesive forces to cause significant deformation of the surface profile. In the JKR regime, the compliance of soft elastomers allows for significant deformation within the contact area to match the rigid indenter profile, and it is such deformation, and the energy dissipated during separation in unstable jumps back to less-deformed states, which generates significant adhesion enhancement.

4. Summary

The mechanics of detachment of a rigid sphere from an axisymmetric wavy surface is analyzed in various adhesion regimes. The JKR solution for the axisymmetric wavy surface contact problem is presented in a new dimensionless form which allows comprehensive adhesion maps to be drawn. It is shown that, if the contact is complete initially over a finite area, then waviness can cause interface toughening via energy dissipation due to instabilities in the detachment load curve, and interface strengthening in the form of higher pull-off forces due to oscillations on the load curves is also observed. These effects can be significant for the soft elastomers where the JKR theory of adhesion is most applicable. To study the effect of surface waviness on stiffer elastic solids, the JKR–DMT transition solution is derived using a Maugis–Dugdale cohesive zone formulation, and the enhancement in adhesion is mapped. It is seen that the presence of surface waviness does not enhance adhesion in the DMT regime, where the surfaces are too rigid to deform significantly enough to generate the instabilities and energy dissipation upon separation that characterizes the adhesion enhancement during detachment in the JKR regime. These analytical results for an idealized wavy surface provide important insights into current models of rough surface adhesion. There is much potential for further experimental work at a variety of length scales to investigate the phenomenon of enhanced adhesion to slightly rough

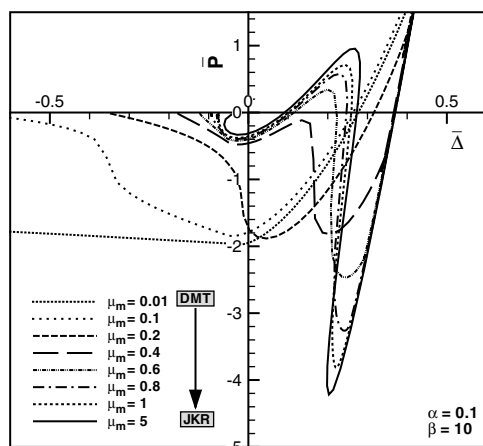


Fig. 9. Representative plot of normal load \bar{P} versus $\bar{\Delta}$ for the Maugis–Dugdale wavy surface adhesion problem, for a range of μ_m within the JKR–DMT transition regime. $\beta = 10$.

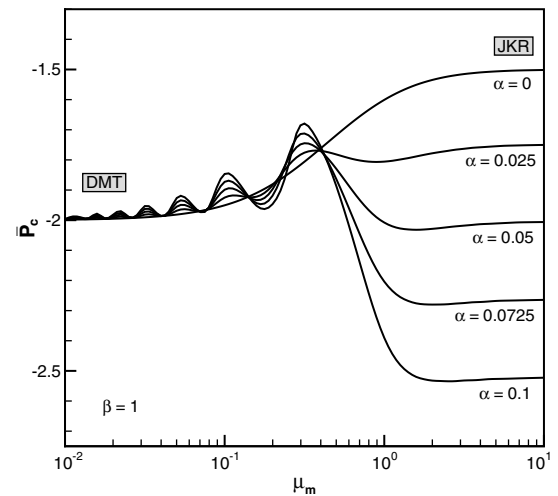


Fig. 10. Map of adhesive pull-off forces \bar{P}_c for the JKR–DMT transition solution for a range of Maugis parameters μ_m , illustrating that adhesion enhancement is limited to the JKR regime. $\beta = 1$.

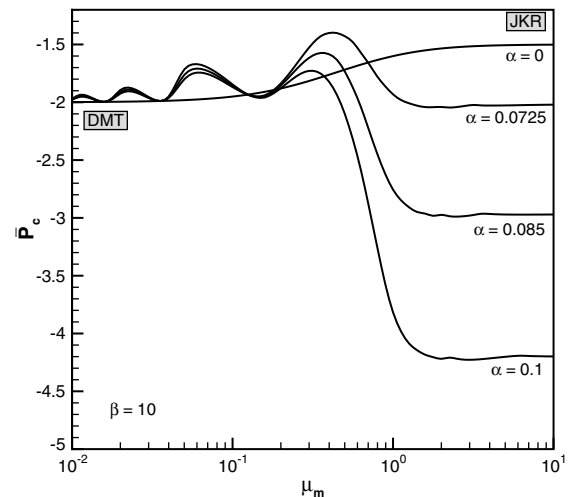


Fig. 11. Map of adhesive pull-off forces \bar{P}_c for the JKR–DMT transition solution for a range of Maugis parameters μ_m , illustrating that adhesion enhancement is limited to the JKR regime. $\beta = 10$.

surfaces in the context of the JKR–DMT transition model presented above, with applications including the optimization of biological adhesion mechanisms and the design of nano- and micro-mechanical devices.

Acknowledgements

This work was supported by grants from the Mechanics of Multifunctional Materials and Microsystems program of the Air Force Office of Scientific Research (Grant # FA9550-05-1-0210, Program Manager: Dr. Les Lee) and the National Science Foundation (# CMS-0547032). JFW acknowledges support from a National Defense Science and Engineering Graduate Fellowship. The authors are grateful for suggestions made by the anonymous reviewers of the original version of this paper.

References

- Abramowitz, M., Stegun, I.A., 1965. Handbook of Mathematical Functions with Formulas, Graphs, and Mathematical Tables. Dover, New York.

- Barquins, M., Maugis, D., 1982. Adhesive contact of axisymmetric punches on an elastic half-space: the modified Hertz–Huber's stress tensor for contacting spheres. *J. Mec. Theor. Appl.* 1, 331–357.
- Barthel, E., 1998. On the description of the adhesive contact of spheres with arbitrary interaction potentials. *J. Colloid Interface Sci.* 200, 7–18.
- Briggs, G.A.D., Briscoe, B.J., 1977. The effect of surface topography on the adhesion of elastic solids. *J. Phys. D Appl. Phys.* 10, 2453–2466.
- Carbone, G., Mangialardi, L., 2004. Adhesion and friction of an elastic half-space in contact with a slightly wavy rigid surface. *J. Mech. Phys. Solids* 52, 1267–1287.
- Derjaguin, B.V., Muller, V.M., Toporov, Y.P., 1975. Effect of contact deformation on the adhesion of particles. *J. Colloid Interface Sci.* 53, 314–326.
- Dugdale, D.S., 1960. Yielding of steel sheets containing slits. *J. Mech. Phys. Solids* 8, 100–104.
- Fuller, K.N.G., Roberts, A.D., 1981. Rubber rolling on rough surfaces. *J. Phys. D Appl. Phys.* 14, 221–239.
- Fuller, K.N.G., Tabor, D., 1975. The effect of surface roughness on the adhesion of elastic solids. *Proc. Roy. Soc. Lond. A* 345, 327–342.
- Greenwood, J.A., Williamson, J.B.P., 1966. Contact of nominally flat surfaces. *Proc. Roy. Soc. Lond. A* 295, 300–319.
- Guduru, P.R., 2007. Detachment of a rigid solid from an elastic wavy surface: theory. *J. Mech. Phys. Solids* 55, 473–488.
- Guduru, P.R., Bull, C., 2007. Detachment of a rigid solid from an elastic wavy surface: experiments. *J. Mech. Phys. Solids* 55, 473–488.
- Hill, R., Storakers, B., 1990. A concise treatment of axisymmetric indentation in elasticity. In: Eason, G., Ogden, R.W. (Eds.), *Elasticity: Mathematical Methods and Applications*. Ellis Horwood Publishers, Chichester, pp. 99–210.
- Hui, C.Y., Lin, Y.Y., Baney, J.M., Kramer, E.J., 2001. The mechanics of contact and adhesion of periodically rough surfaces. *J. Polym. Sci. B Polym. Phys.*, 1196–1214.
- Johnson, K.L., 1985. *Contact Mechanics*. Cambridge University Press, Cambridge.
- Johnson, K.L., 1995. The adhesion of two elastic bodies with slightly wavy surfaces. *Int. J. Solids Struct.* 32, 423–430.
- Johnson, K.L., Greenwood, J.A., 1997. An adhesion map for the contact of elastic spheres. *J. Colloid Interface Sci.* 192, 326–333.
- Johnson, K.L., Kendall, K., Roberts, A.D.R., 1971. Surface energy and the contact of elastic solids. *Proc. Roy. Soc. Lond. A* 324, 301–313.
- Kim, K.-S., McMeeking, R.M., Johnson, K.L., 1998. Adhesion, slip, cohesive zones and energy fluxes for elastic spheres in contact. *J. Mech. Phys. Solids* 46, 243–266.
- Kim, H.-C., Russell, T.P., 2001. Contact of elastic solids with rough surfaces. *J. Polym. Sci. B Polym. Phys.* 39, 1848–1854.
- Maugis, D., 1992. Adhesion of spheres: the JKR–DMT transition using a Dugdale model. *J. Colloid Interface Sci.* 150, 243–269.
- Maugis, D., 2000. *Contact, Adhesion, and Rupture of Elastic Solids*. Springer, Berlin.
- Morrow, C.A., Lovell, M.R., 2005. A solution for lightly loaded adhesive rough surfaces with application to MEMS. *Trans. ASME J. Tribol.* 127, 206–212.
- Morrow, C., Lovell, M., Ning, X., 2003. A JKR–DMT transition solution for adhesive rough surface contact. *J. Phys. D Appl. Phys.* 36, 534–540.
- Muller, V.M., Yushenko, V.S., Derjaguin, B.V., 1980. On the influence of molecular forces on the deformation of an elastic sphere and its sticking to a rigid plane. *J. Colloid Interface Sci.* 77, 91–101.
- Muller, V.M., Derjaguin, B.V., Toporov, Y.P., 1983. On two methods of calculation of the force of sticking of an elastic sphere to a rigid plane. *Colloids Surf.* 7, 251–259.
- Persson, B.N.J., 2002. Adhesion between an elastic body and a randomly rough hard surface. *Eur. Phys. J. E8*, 385–401.
- Persson, B.N.J., Tosatti, E., 2001. The effect of surface roughness on the adhesion of elastic solids. *J. Chem. Phys.* 115, 5597–5610.
- Santos, R., Gorb, S., Jamar, V., Flammang, P., 2005. Adhesion of echinoderm tube feet to rough surfaces. *J. Exp. Biol.* 208, 2555–2567.
- Shi, X., Polycarpou, A.A., 2005. Adhesive transition from noncontacting to contacting elastic spheres: extension of the Maugis–Dugdale model. *J. Colloid Interface Sci.* 281, 449–457.
- Sneddon, I.N., 1965. The relation between load and penetration in the axisymmetric Boussinesq problem for a punch of arbitrary profile. *Int. J. Eng. Sci.* 3, 47–56.
- Tabor, D., 1977. Surface forces and surface interactions. *J. Colloid Interface Sci.* 58, 2–13.
- Walker, G., 1987. Marine organisms and their adhesion. In: Wake, W.C. (Ed.), *Synthetic Adhesives and Sealants*. John Wiley & Sons, Chichester.
- Zilberman, S., Persson, B.N.J., 2002. Adhesion between elastic bodies with rough surfaces. *Solid State Commun.* 123, 173–177.